ISBN: 978-3-95450-262-2 ISSN: 2673-5350 doi: 10.18429/JACoW-IBIC2025-TUPMO26

ELECTRON BEAM ENERGY MEASUREMENT IN THE SLRI 6 MeV LINAC USING X-RAY SCINTILLATOR IMAGING

P. Boonpornprasert, J. Nadeedanklang, N. Yachum, D. Khampiranon,
K. Manasatitpong, S. Kokkrathoke, T. Chanwattana, S. Chunjarean *
Synchrotron Light Research Institute, Muang District, Nakhon Ratchasima, Thailand

Abstract

The Synchrotron Light Research Institute (SLRI) in Thailand aims to operate a 6 MeV electron linear accelerator for irradiation, supporting various agricultural and industrial applications. This study presents a method for measuring the electron beam energy using the existing dipole magnet in the beamline, originally designed to scan X-rays on samples through a scan horn. An aluminum sheet coated with terbium-doped gadolinium oxysulfide (Gd_2O_2S) was used as a scintillation screen for X-ray imaging and placed downstream of the scan horn. X-ray scintillator images were captured with a CCD camera. By analyzing shifts in the X-ray image centroid as the dipole magnet current varied, the electron beam energy was determined.

INTRODUCTION

Electron linear accelerators (linacs) with energies from a few to tens of MeV are used for applications such as medical sterilization and agricultural irradiation [1]. The Synchrotron Light Research Institute (SLRI) has developed a 6 MeV linac for irradiating fresh fruit [2], an application where the beam energy is an important parameter for effective sterilization.

Figure 1 shows the layout of the linac. Its main components are a thermionic cathode DC gun, a side-coupling S-band linac, a beam current monitor (ACCT), a vacuum chamber and bellow for beam transport, a scanning magnet, a scan horn, and finally, a tungsten target. The electrons produce X-rays upon hitting the target, and these X-rays are used to irradiate samples. The distances from the linac exit to the tungsten target and the sample irradiation area are approximately 1.0 m and 1.3 m, respectively. Table 1 summarizes the operational parameters of the system. Further details on the control and timing systems are described elsewhere in [3, 4].

A measurement of the beam energy is necessary for proper operation. Typically, this measurement requires a dipole magnet and a screen to observe the electron beam directly. Since the linac beamline lacks a dedicated screen, this study introduces an indirect measurement method. The existing scanning magnet shifts the position of the electron beam on the tungsten target, which consequently shifts the location of the X-ray source. By imaging the X-rays with a scintillator, we can determine the beam energy from the relationship between the magnet current and the position of the X-ray spot. This method avoids installing additional in-vacuum hardware. This paper presents the configuration, simulation, and results of this measurement.

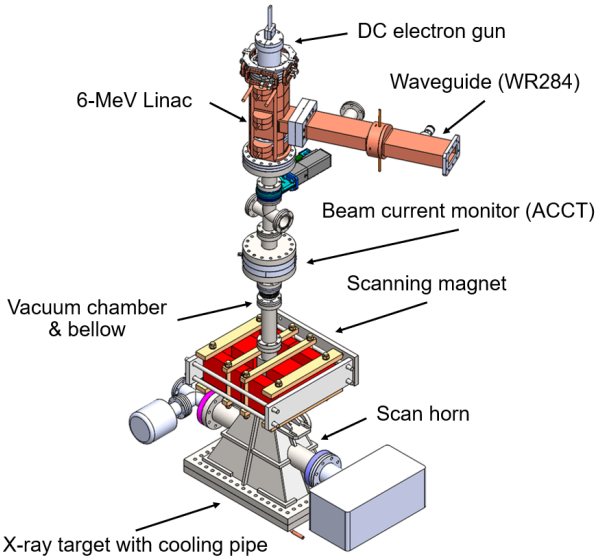

Figure 1: Layout of the 6 MeV linac at SLRI.

Table 1: Operational Parameters of the 6-MeV Linac System

Parameters	Details
Gun cathode filament voltage	4.4-4.6 V
Gun modulator voltage	950 V
Gun modulator pulse width	5 µs
RF modulator voltage	1043 V
RF peak power	3.2 MW
RF pulse repetition rate	100-200 Hz
RF macropulse width	5-10 µs
Linac resonance frequency	2.998 GHz
Beam average current	130 mA

CONFIGURATION FOR BEAM ENERGY MEASUREMENT

The principle used for beam energy measurement is illustrated in Fig. 2. The electron beam, after passing through the linac and scanning magnet, strikes a composite X-ray target located at the end of the scan horn. The target is designed for both efficient Bremsstrahlung conversion and thermal stability. It consists of a 0.8 mm thick tungsten sheet brazed to an Oxygen-Free High-Conductivity (OFHC) copper substrate. Tungsten was selected for its high atomic number (Z), which

* somjai@slri.or.th

ISBN: 978-3-95450-262-2 ISSN: 2673-5350 doi: 10.18429/JACoW-IBIC2025-TUPMO26

maximizes the X-ray yield. The copper substrate provides high thermal conductivity to dissipate heat from the focal point, while the brazing ensures good thermal contact and structural integrity.

A scintillator screen is placed near the tungsten sheet to detect the resulting X-rays. This screen is made of an aluminum sheet with a 5 mm × 5 mm grid pattern and coated with Gd_2O_2S along these grid lines. When the electrons impact the tungsten target, they produce Bremsstrahlung X-rays, which excite the scintillator and emit visible light. This light is reflected by a mirror and captured by a CCD camera.

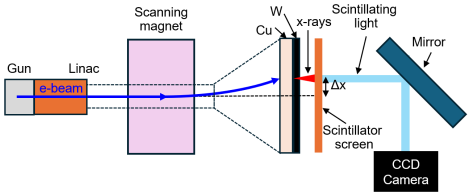

Figure 2: Configuration layout for beam energy measurement using Bremsstrahlung X-rays and scintillator detection.

The scanning magnet used in this setup is an H-shaped dipole magnet manufactured at SLRI. It has an effective magnetic length of 148 mm. The relationship between its magnetic field strength B_y (in mT) and the applied current I (in A), was determined with Hall probe measurements and is given by:

$$B_y = 4.69I - 0.0427. \quad (1)$$

By varying the current supplied to the scanning magnet, the average impact position of the electron beam on the target is shifted by a displacement Δx. This displacement is dependent on both the beam energy and the magnet current. Beam dynamics simulations can be used to determine how Δx changes with current for different beam energies, which provides a basis for beam energy calibration.

SIMULATION OF MEASUREMENT

Beam dynamics simulations were performed using ASTRA [5]. These simulations modeled the beam energy measurement by tracking an initial electron bunch with an average current of 130 mA from the cathode to the scan horn exit. Figure 3 shows the final average transverse beam position as a function of scanning magnet current for each simulated beam kinetic energy. Linear regressions of these plots yielded slopes, which were then plotted as a function of beam kinetic energy in Fig. 4. The slope uncertainties (horizontal error bars) were derived from the linear fits. An exponential fit to these data points produced the equation:

$$y = (19.56)e^{-0.12x} + 1.26, \quad (2)$$

where y is the beam kinetic energy and x is the slope. To simplify the analysis, it was assumed that the electron beam transverse profile is identical to the X-ray scintillation image, and that the thicknesses of the copper and tungsten sheets are negligible. Under these assumptions, Eq. (2) can be used to determine the beam's kinetic energy from experimental slope measurements of the X-ray scintillation image shifts.

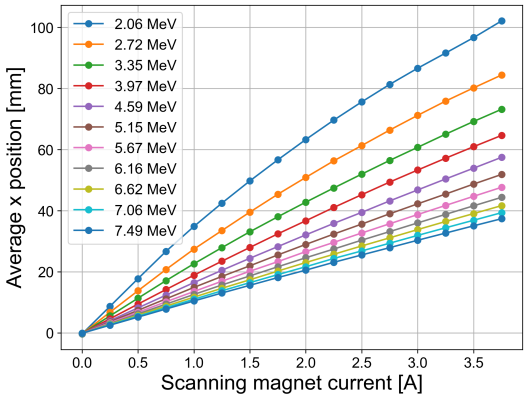

Figure 3: Average transverse beam position as a function of the scanning magnet current for various simulated beam kinetic energies.

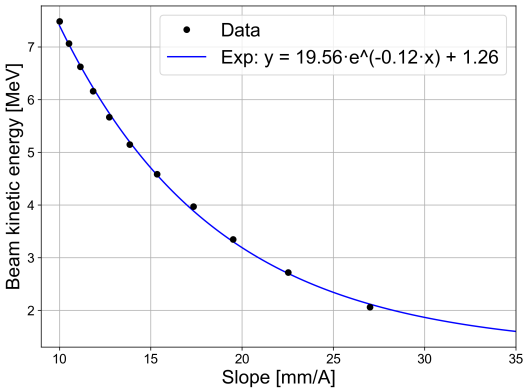

Figure 4: The simulated beam kinetic energy as a function of slopes of the linear regressions from Fig. 3. The blue line is the exponential fit according to Eq 2.

BEAM ENERGY MEASUREMENTS

To measure beam energy, the RF modulator voltage (HV), which controls the RF of the linac, was varied from 900 V to 1080 V, generating different beam kinetic energies. At each HV setting, the scanning magnet current was adjusted from -4 A to 4 A with 0.5 A steps, and the resulting X-ray image from the scintillator was recorded. The recorded images were then processed using Python scripts. A rectangular region of interest (ROI) was manually selected around the X-ray profile, and a median filter and thresholding were applied to reduce noise. The horizontal projection of the processed image was then computed to create a histogram, as shown in the example in Fig. 5. A calibration factor (mm/pixel) was calculated from the known 5 mm separation of the peaks in

ISBN: 978-3-95450-262-2 ISSN: 2673-5350 doi: 10.18429/JACoW-IBIC2025-TUPMO26

the histogram, allowing for the conversion from pixels to metric units. Figure 6 shows the average x position of the X-ray profile as a function of the scanning magnet current at the HV of 1043 V. A linear fit to this data provides a slope, which for this example is 17.55 mm/A with an uncertainty of 0.30 mm/A. This uncertainty combines the standard error from the fit and the limits of the pixel resolution.

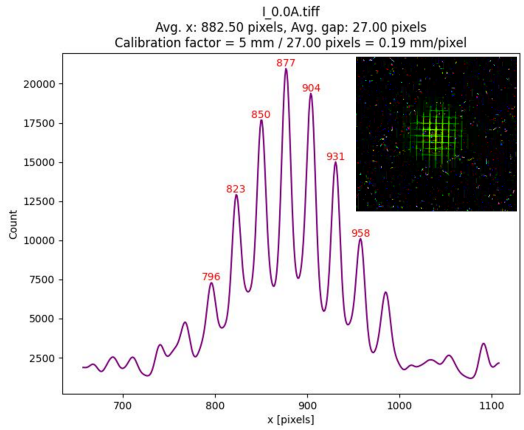

Figure 5: Example of a recorded scintillating X-ray image and its processed projection histogram. The inset shows the raw image (HV = 1043 V, magnet current = 0 A), and the main plot shows the horizontal (x) projection histogram after ROI selection, filtering, and thresholding.

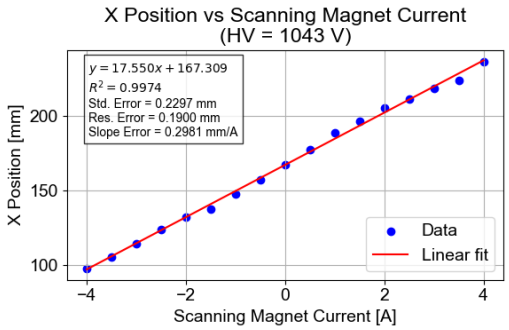

Figure 6: Average horizontal (x) position of the X-ray image as a function of scanning magnet current at a high voltage (HV) of 1043 V, with the linear fit used to determine the slope.

This procedure was repeated for each HV setting to determine the slope and its associated uncertainty. Using the assumptions from the previous section, these slope values were used in Eq. (2) to calculate the beam kinetic energy. Figure 7 plots the calculated beam kinetic energies against the corresponding HV settings. The plot shows a general trend of increasing kinetic energy with increasing HV. The measured beam kinetic energy ranged from approximately 1.8 MeV at the lowest HV setting of 900 V to a maximum of 4.31 MeV at the highest HV setting of 1080 V.

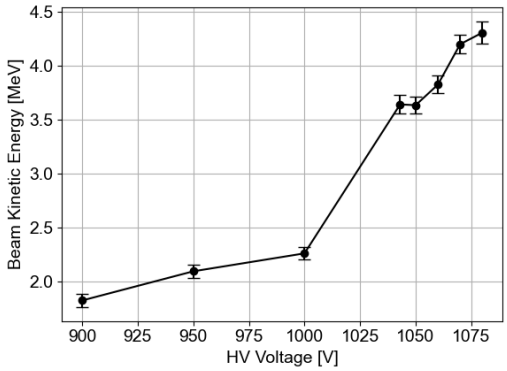

Figure 7: Measured beam kinetic energy as a function of modulator high voltage (HV).

The measured maximum energy of 4.31 MeV is substantially lower than the 6 MeV design value, which has significant consequences for the fruit irradiation application. The kinetic energy of the electron beam determines the endpoint energy of the resulting Bremsstrahlung X-ray spectrum, which in turn dictates the penetration capability of the X-rays. A reduction in beam energy from 6 MeV to 4.31 MeV produces a less penetrating X-ray field. This may compromise the ability to deliver a sufficient radiation dose to the center of larger or denser products, limiting the effective range of products for sterilization. Furthermore, the lower beam energy reduces the overall dose rate, which requires longer exposure times to achieve the target dose and therefore decreases the operational throughput of the facility.

CONCLUSION

This paper has presented a method for measuring the energy of the electron beam in the 6 MeV linac at SLRI using X-ray scintillator imaging with a scanning magnet. The maximum measured kinetic energy was 4.31 MeV, which is lower than the design value of 6 MeV.

To enhance the performance of the linac and reconcile the observed energy with the design value, a detailed investigation correlating the input RF power with the resulting beam energy is required. Furthermore, the accuracy of the energy measurement itself could be improved by refining the underlying model. Future studies should address the assumptions made in this work, including a quantitative analysis of the relationship between the electron beam profile and the measured X-ray scintillation image. Additionally, the energy loss of the electron beam within the target materials, which was ignored in the present analysis, must be accounted for in future work. For instance, the calculation should include the total mass stopping power of the copper substrate.

ACKNOWLEDGEMENTS

The authors wish to thank SLRI staff for their assistance and support. Funding for this research was granted by the Program Management Unit for Human Resources and Institutional Development, Research and Innovation (PMU-B).

ISBN: 978-3-95450-262-2 ISSN: 2673-5350 doi: 10.18429/JACoW-IBIC2025-TUPMO26

REFERENCES

[1] S. Hanna, *RF Linear Accelerators for Medical and Industrial Applications*. Boston, MA, USA, Artech House, 2012.

[2] S. Chunjarean *et al.*, "Development of a 6 MeV Electron Beam Energy Linac for Fruit Sterilization", *J. Phys.: Conf. Ser.*, vol. 2431, p. 012071, 2023. doi:10.1088/1742-6596/2431/1/012071

[3] N. Yachum, S. Chunjarean, N. Russamee, and J. Srisertpol, "Parameter Optimization of Hole-Slot-Type Magnetron for Controlling Resonant Frequency of Linear Accelerator 6 MeV by Reverse Engineering Technique", *Appl. Sci.*, vol. 11, p. 2384, 2021. doi:10.3390/app11052384

[4] S. Kokkrathoke, N. Yachum, S. Chunjarean, and K. Manasatitpong, "Synchronisation of Linear Accelerator for Fruit Irradiation with FPGA-Based System", *J. Phys.: Conf. Ser.*, vol. 2653, p. 012028, 2023. doi:10.1088/1742-6596/2653/1/012028

[5] K. Floettmann, *A Space Charge Tracking Algorithm*, DESY, Germany, 2017. https://www.desy.de/~mpyflo/